Research Article | Vol. 25, No. 2 | 23 Jan 2017 | OPTICS EXPRESS 1542
Optics EXPRESS

Two-octave spanning supercontinuum generation in stoichiometric silicon nitride waveguides pumped at telecom wavelengths

MARCO A. G. PORCEL,[1,6] FLORIAN SCHEPERS,[2,6] JÖRN P. EPPING,[1] TIM HELLWIG,[2] MARCEL HOEKMAN,[3] RENÉ G. HEIDEMAN,[3] PETER J. M. VAN DER SLOT,[1,*] CHRIS J. LEE,[4] ROBERT SCHMIDT,[5], RUDOLF BRATSCHITSCH,[5] CARSTEN FALLNICH,[1,2] AND KLAUS-J. BOLLER[1]

[1]*Laser Physics and Nonlinear Optics Group, MESA+ Institute for Nanotechnology, University of Twente, P.O. Box 217, Enschede 7500 AE, The Netherlands*
[2]*Institute of Applied Physics, Westfälische Wilhelms-Universität, Corrensstrasse 2, 48149 Münster, Germany*
[3]*LioniX International B.V., PO Box 456, Enschede 7500 AL, The Netherlands*
[4]*XUV Optics group, MESA+ Institute for Nanotechnology, University of Twente, P.O. Box 217, Enschede 7500 AE, The Netherlands*
[5]*Institute of Physics, Westfälische Wilhelms-Universität, Wilhelm-Klemm-Str. 10, 48149 Münster, Germany*
[6]*These authors contributed equally to this work*
[*]*p.j.m.vanderslot@utwente.nl*

Abstract: We demonstrate supercontinuum generation in stoichiometric silicon nitride (Si_3N_4 in SiO_2) integrated optical waveguides, pumped at telecommunication wavelengths. The pump laser is a mode-locked erbium fiber laser at a wavelength of 1.56 μm with a pulse duration of 120 fs. With a waveguide-internal pulse energy of 1.4 nJ and a waveguide with 1.0 μm x 0.9 μm cross section, designed for anomalous dispersion across the 1500 nm telecommunication range, the output spectrum extends from the visible, at around 526 nm, up to the mid-infrared, at least to 2.6 μm, the instrumental limit of our detection. This output spans more than 2.2 octaves (454 THz at the -30 dB level). The measured output spectra agree well with theoretical modeling based on the generalized nonlinear Schrödinger equation. The infrared part of the supercontinuum spectra shifts progressively towards the mid-infrared, well beyond 2.6 μm, by increasing the width of the waveguides.

OCIS codes: (130.0130) Integrated optics; (190.4390) Nonlinear optics, integrated optics; (320.6629) Supercontinuum generation; (190.7110) Ultrafast nonlinear optics.

References and links

1. J. M. Dudley, G. Genty, and S. Coen, "Supercontinuum generation in photonic crystal fiber," Rev. Mod. Phys. **78**, 1135–1184 (2006).
2. D. J. Jones, S. A. Diddams, J. K. Ranka, A. Stentz, R. S. Windeler, J. L. Hall, and S. T. Cundiff, "Carrier-Envelope Phase Control of Femtosecond Mode-Locked Lasers and Direct Optical Frequency Synthesis," Science **288**, 635–639 (2000).
3. A. Ruehl, M. J. Martin, K. C. Cossel, L. Chen, H. McKay, B. Thomas, C. Benko, L. Dong, J. M. Dudley, M. E. Fermann, I. Hartl, and J. Ye, "Ultrabroadband coherent supercontinuum frequency comb," Phys. Rev. A **84**, 011806 (2011).
4. H. Kano and H. Hamaguchi, "Characterization of a supercontinuum generated from a photonic crystal fiber and its application to coherent Raman spectroscopy," Opt. Lett. **28**, 2360–2362 (2003).
5. G. Humbert, W. Wadsworth, S. Leon-Saval, J. Knight, T. Birks, P. St. J. Russell, M. Lederer, D. Kopf, K. Wiesauer, E. Breuer, and D. Stifter, "Supercontinuum generation system for optical coherence tomography based on tapered photonic crystal fibre," Opt. Express **14**, 1596–1603 (2006).
6. J. T. Woodward, A. W. Smith, C. A. Jenkins, C. Lin, S. W. Brown, and K. R. Lykke, "Supercontinuum sources for metrology," Metrologia **46**, S277–S282 (2009).

#281693 http://dx.doi.org/10.1364/OE.25.001542
Journal © 2017 Received 28 Nov 2016; revised 6 Jan 2017; accepted 8 Jan 2017; published 19 Jan 2017

Optics EXPRESS

7. G. Ycas, S. Osterman, and S. A. Diddams, "Generation of a 660–2100 nm laser frequency comb based on an erbium fiber laser," Opt. Lett. **37**, 2199–2201 (2012).
8. V. Brasch, T. Herr, M. Geiselmann, G. Lihachev, M. H. P. Pfeiffer, M. L. Gorodetsky, and T. J. Kippenberg, "Photonic chip based optical frequency comb using soliton induced Cherenkov radiation," Science **351**, 357–360 (2016).
9. V. Torres-Company and A. M. Weiner, "Optical frequency comb technology for ultra-broadband radio-frequency photonics," Laser Photonics Rev. **8**, 368–393 (2014).
10. T. G. Nguyen, M. Shoeiby, S. T. Chu, B. E. Little, R. Morandotti, A. Mitchell, and D. J. Moss, "Integrated frequency comb source based Hilbert transformer for wideband microwave photonic phase analysis," Opt. Express **23**, 22087–22097 (2015).
11. K.L. Corwin, N.R. Newbury, J.M. Dudley, S. Coen, S.A. Diddams, K. Weber, and R.S. Windeler, "Fundamental Noise Limitations to Supercontinuum Generation in Microstructure Fiber," Phys. Rev. Lett. **90**, 113904 (2003).
12. B. Kuyken, F. Leo, S. Clemmen, U. Dave, R. Van Laer, T. Ideguchi, H. Zhao, X. Liu, J. Safioui, S. Coen, S.P. Gorza, S.K. Selvaraja, S. Massar, R.M. Osgood Jr., P. Verheyen, J. Van Campenhout, R. Baets, W.M.J. Green, G. Roelkens, "Nonlinear optical interactions in silicon waveguides," Nanophotonics **5**, 1–16 (2016).
13. C. Ciret and S-P. Gorza, "Generation of ultra broadband coherent supercontinuum in tapered and dispersion managed silicon nanophotonic waveguides," arXiv:1610.05665 [physics.optics] (2016).
14. H. Hu, W. Li, N.K. Dutta, "Dispersion-engineered tapered planar waveguide for coherent supercontinuum generation," Opt. Commun. **324**, 252–257 (2014).
15. D. Y. Oh, D. Sell, H. Lee, K. Y. Yang, S. A. Diddams, and K. J. Vahala, "Supercontinuum generation in an on-chip silica waveguide," Opt. Lett. **39**, 1046–1048 (2014).
16. D. Duchesne, M. Peccianti, M. R. E. Lamont, M. Ferrera, L. Razzari, F. Légaré, R. Morandotti, S. Chu, B. E. Little, and D. J. Moss, "Supercontinuum generation in a high index doped silica glass spiral waveguide," Opt. Express **18**, 923–930 (2010).
17. R. Halir, Y. Okawachi, J. S. Levy, M. A. Foster, M. Lipson, and A. L. Gaeta, "Ultrabroadband supercontinuum generation in a CMOS-compatible platform," Opt. Lett. **37**, 1685–1687 (2012).
18. J. M. Chavez Boggio, D. Bodenmüller, T. Fremberg, R. Haynes, M. M. Roth, R. Eisermann, M. Lisker, L. Zimmermann, and M. Böhm, "Dispersion engineered silicon nitride waveguides by geometrical and refractive-index optimization," J. Opt. Soc. Am. B **31**, 2846–2857 (2014).
19. M. R. Lamont, B. Luther-Davies, D.-Y. Choi, S. Madden, and B. J. Eggleton, "Supercontinuum generation in dispersion engineered highly nonlinear (γ = 10 /W/m) As_2S_3 chalcogenide planar waveguide," Opt. Express **16**, 14938–14944 (2008).
20. Y. Yu, X. Gai, P. Ma, D.-Y. Choi, Z. Yang, R. Wang, S. Debbarma, S. J. Madden, and B. Luther-Davies, "A broadband, quasi-continuous, mid-infrared supercontinuum generated in a chalcogenide glass waveguide," Laser Photonics Rev. **8**, 792–798 (2014).
21. F. Leo, S.-P. Gorza, J. Safioui, P. Kockaert, S. Coen, U. Dave, B. Kuyken, and G. Roelkens, "Dispersive wave emission and supercontinuum generation in a silicon wire waveguide pumped around the 1550 nm telecommunication wavelength," Opt. Lett. **39**, 3623–3626 (2014).
22. R. K. W. Lau, M. R. E. Lamont, A. G. Griffith, Y. Okawachi, M. Lipson, and A. L. Gaeta, "Octave-spanning mid-infrared supercontinuum generation in silicon nanowaveguides," Opt. Lett. **39**, 4518–4521 (2014).
23. B. Kuyken, T. Ideguchi, S. Holzner, M. Yan, T. W. Hänsch, J. Van Campenhout, P. Verheyen, S. Coen, F. Leo, R. Baets, G. Roelkens, and N. Picqué, "An octave-spanning mid-infrared frequency comb generated in a silicon nanophotonic wire waveguide," Nat. Commun. **6**, 6310 (2015).
24. X. Liu, M. Pu, B. Zhou, C. J. Krückel, A. Fülöp, V. Torres-Company, and M. Bache, "Octave-spanning supercontinuum generation in a silicon-rich nitride waveguide," Opt. Lett. **41**, 2719–2722 (2016).
25. F. Morichetti, A. Melloni, M. Martinelli, R. Heideman, A. Leinse, D. Geuzebroek, and A. Borremann, "Box-shaped dielectric waveguides: A new concept in integrated optics?" J. Lightwave Technol. **25**, 2579–2589 (2007).
26. R. G. H. Kerstin Wörhoff, "TriPleX: A versatile dielectric photonic platform," Adv. Opt. Techn. **4**, 189–207 (2015).
27. R. M. Oldenbeuving, E. J. Klein, H. L. Offerhaus, C. J. Lee, H. Song, and K.-J. Boller, "25 kHz narrow spectral bandwidth of a wavelength tunable diode laser with a short waveguide-based external cavity," Laser Phys. Lett. **10**, 015804 (2013).
28. Y. Fan, R. M. Oldenbeuving, E. J. Klein, C. J. Lee, H. Song, M. R. H. Khan, H. L. Offerhaus, P. J. M. van der Slot, and K.-J. Boller, "A hybrid semiconductor-glass waveguide laser," Proc. SPIE **9135**, 91351 (2014).
29. A. Gondarenko, J. S. Levy, and M. Lipson, "High confinement micron-scale silicon nitride high Q ring resonator," Opt. Express **17**, 11366–11370 (2009).
30. J. F. Bauters, M. J. R. Heck, D. John, D. Dai, M.-C. Tien, J. S. Barton, A. Leinse, R. G. Heideman, D. J. Blumenthal, and J. E. Bowers, "Ultra-low-loss high-aspect-ratio Si_3N_4 waveguides," Opt. Express **19**, 3163-3174 (2011).
31. C. Xiong, X. Zhang, A. Mahendra, J. He, D.-Y. Choi, J. Chae, D. Marpaung, A. Leinse, R. G. Heideman, M. Hoekman, C. G. H. Roeloffzen, R. M. Oldenbeuving, P. W. L. van Dijk, C. Taddei, P. H. W. Leong, and B. J. Eggleton, "Compact and reconfigurable silicon nitride time-bin entanglement circuit," Optica **2**, 724–727 (2015).
32. L. Zhuang, D. Marpaung, M. Burla, W. Beeker, A. Leinse, and C. Roeloffzen, "Low-loss, high-index-contrast Si_3N_4/SiO_2 optical waveguides for optical delay lines in microwave photonics signal processing," Opt. Express **19**, 23162–23170 (2011).
33. C. G. H. Roeloffzen, L. Zhuang, C. Taddei, A. Leinse, R. G. Heideman, P. W. L. van Dijk, R. M. Oldenbeuving,

D. A. I. Marpaung, M. Burla, and K. J. Boller, "Silicon nitride microwave photonic circuits," Opt. Express **21**, 22937–22961 (2013).
34. L. Zhuang, C. G. H. Roeloffzen, M. Hoekman, K.-J. Boller, and A. J. Lowery, "Programmable photonic signal processor chip for radiofrequency applications," Optica **2**, 854–859 (2015).
35. A. Klenner, A.S. Mayer, A.R. Johnson, K. Luke, M.R.E. Lamont, Y. Okawachi,M. Lipson, A.L. Gaeta, and U. Keller, "Gigahertz frequency comb offset stabilization based on supercontinuum generation in silicon nitride waveguides," Opt. Express **24**, 11043–11053 (2016).
36. J. P. Epping, T. Hellwig, M. Hoekman, R. Mateman, A. Leinse, R. G. Heideman, A. van Rees, P. J. M. van der Slot, C. J. Lee, C. Fallnich, and K.-J. Boller, "On-chip visible-to-infrared supercontinuum generation with more than 495 THz spectral bandwidth," Opt. Express **23**, 19596–19604 (2015).
37. A.R. Johnson, A.S. Mayer, A. Klenner, K. Luke, E.S. Lamb, M.R.E. Lamont, C. Joshi, Y. Okawachi, F.W. Wise, M. Lipson, U. Keller, and A.L. Gaeta, "Octave-spanning coherent supercontinuum generation in a silicon nitride waveguide," Opt. Lett. **40**, 5117–5120, (2015).
38. A.S. Mayer, A. Klenner, A.R. Johnson, K. Luke, M.R.E. Lamont, Y. Okawachi, M. Lipson, A.L. Gaeta, and U. Keller, "Frequency comb offset detection using supercontinuum generation in silicon nitride waveguides," Opt. Express **23**, 15440–15451 (2015).
39. G. P. Agrawal, *Nonlinear Fiber Optics* (Academic Press, 2007).
40. J. P. Epping, M. Hoekman, R. Mateman, A. Leinse, R. G. Heideman, A. van Rees, P. J. van der Slot, C. J. Lee, and K.-J. Boller, "High confinement, high yield Si_3N_4 waveguides for nonlinear optical applications," Opt. Express **23**, 642–648 (2015).
41. K. Luke, Y. Okawachi, M. R. E. Lamont, A. L. Gaeta, and M. Lipson, "Broadband mid-infrared frequency comb generation in a Si_3N_4 microresonator," Opt. Lett. **40**, 4823–4826 (2015).
42. M. Kues, N. Brauckmann, T. Walbaum, P. Groß, and C. Fallnich, "Nonlinear dynamics of femtosecond supercontinuum generation with feedback," Opt. Express **17**, 15827–15841 (2009).
43. J.S. Levy, *Integrated nonlinear optics in silicon nitride waveguides resonators*, PhD Thesis, Cornell University (2011).
44. K. Ikeda, R. E. Saperstein, N. Alic, and Y. Fainman, "Thermal and Kerr nonlinear properties of plasma-deposited silicon nitride/ silicon dioxide waveguides," Opt. Express **16**, 12987–12994 (2008).
45. X.-J. Liu, J.-J. Zhang, X.-W. Sun, Y.-B. Pan, L.-H. Huang, and C.-Y. Jin, "Growth and properties of silicon nitride films prepared by low pressure chemical vapor deposition using trichorosilane and ammonia," Thin Solid Films **460**, 72–77 (2004).
46. C. Krueckel, A. Fulop, T. Klintberg, J. Bengtsson, P. Andrekson, and V. Torres-Company, "Linear and nonlinear characterization of low-stress high-confinement silicon-rich nitride waveguides," Opt. Express **23**, 25827–25837 (2015).
47. H. Zhao, B. Kuyken, S. Clemmen, F. Leo, A. Subramanian, A. Dhakal, P. Helin, S. Severi, E. Brainis, G. Roelkens, and R. Baets, "Visible-to-near-infrared octave spanning supercontinuum generation in a silicon nitride waveguide," Opt. Lett. **40**, 2177–2180 (2015).
48. N. Karasawa, S. Nakamura, N. Nakagawa, M. Shibata, R. Morita, H. Shigekawa, and M. Yamashita, "Comparison between theory and experiment of nonlinear propagation for a-few-cycle and ultrabroadband optical pulses in a fused silica fiber," IEEE J. Sel. Top. Quantum Electron. **37**, 398–404 (2001).
49. J. M. C. Boggio, A. O. M. Moñux, D. Modotto, T. Fremberg, D. Bodenmüller, D. Giannone, M. M. Roth, T. Hansson, S. Wabnitz, E. Silvestre, and L. Zimmermann, "Dispersion-optimized multicladding silicon nitride waveguides for nonlinear frequency generation from ultraviolet to mid-infrared," J. Opt. Soc. Am. B **33**, 2402–2413 (2016).
50. J.P. Epping, *Dispersion engineering silicon nitride waveguides for broadband nonlinear frequency conversion*, PhD thesis, University of Twente (2015)
51. N. Akhmediev and M. Karlsson, "Cherenkov radiation emitted by solitons in optical fibers," Phys. Rev. A **51**, 2602–2607 (1995).
52. I. Cristiani, R. Tediosi, L. Tartara, and V. Degiorgio, "Dispersive wave generation by solitons in microstructured optical fibers," Opt. Express **12**, 124–135 (2004).
53. F. Schepers, M. A. G. Porcel, J. P. Epping, T. Hellwig, M. Hoekman, R. Mateman, A. Leinse, R. G. Heideman, A. van Rees, P. J. M. van der Slot, C. J. Lee, R. Schmidt, R. Bratschitsch, K.-J. Boller, and C. Fallnich, "Ultra-broadband supercontinuum generation at telecommunication wavelengths in dispersion engineered stoichiometric Si_3N_4 waveguides," in "Conference on Lasers and Electro-Optics," (Optical Society of America, 2016), p. AM3J.5.
54. D. Grassani, A. Billat, M. H. P. Pfeiffer, H. Guo, T. North, T. J. Kippenberg, and C.-S. Bres, "Mid-infrared supercontinuum generation in a SiN waveguide pumped at 1.55 micron," in "Frontiers in Optics 2016," (Optical Society of America, 2016), p. FTu5D.3.
55. B.-H. Liao and C.-N. Hsiao, "Improving optical properties of silicon nitride films to be applied in the middle infrared optics by a combined high-power impulse/unbalanced magnetron sputtering deposition technique," Appl. Opt. **53**, A377–A382 (2014).
56. A. H. Hosseinnia, A. H. Atabaki, A. A. Eftekhar, and A. Adibi, "High-quality silicon on silicon nitride integrated optical platform with an octave-spanning adiabatic interlayer coupler," Opt. Express **23**, 30297-30307 (2015).
57. Y.K. Chembo, "Kerr optical frequency combs: theory, applications and perspectives," Nanophotonics, **5**, 214–230 (2016).

Optics EXPRESS

58. A. Schliesser, N. Picqué, and T.W. Hänsch, "Mid-infrared frequency combs," Nat. Photonics **6**, 440–449 (2012).

1. Introduction

Supercontinuum generation (SCG), typically obtained with femtosecond pulses in photonic crystal fibers [1], is a powerful method of providing extremely broadband spectra with full spatial and temporal coherence [2, 3]. Such nonlinear optical generation is of high interest for numerous applications, for instance in spectroscopy [4], with visible wavelengths in the life sciences [5], or in precision metrology [2,6]. In addition, there is a growing relevance for coherent on-chip generation of broadband light based on lasers in the telecommunication wavelength range [7]. Envisioned applications include chip-sized frequency combs [8] or wideband integrated microwave photonics [9, 10].

Using standard photonic crystal fibers, which typically requires interaction lengths of tens of centimeters for efficient SCG, provides considerable design flexibility in their dispersive and nonlinear properties [1]. However, the shot-to-shot coherence of the SC output decreases with increasing pump pulse duration as well as with the interaction length [1, 11], particularly in the presence of Raman scattering [11]. In contrast, the conversion of ultra-short pulses (< 100 fs) remains coherent in short fibers, but the conversion remains inefficient with a short interaction length. Employing integrated optical waveguides on a chip provides the advantage of tight mode confinement which strongly increases the nonlinear coefficient. This enables an efficient conversion of ultrashort pulses also with short interaction lengths while preserving coherence. For instance, pulses with up to a few hundred femtoseconds have been used for efficient SCG in short optical waveguides while maintaining a high degree of coherence [12–14]. As a second advantage the integrated optical approach offers a route for high-volume and low-cost fabrication, in particular when the waveguide platform is compatible with metal-oxide-semiconductor (CMOS) fabrication facilities.

Lasers in the telecom range, due to their wide availability and maturity, have been employed for SCG in a variety of photonic platforms that are compatible with CMOS fabrication facilities. Examples are doped silica ridge waveguides using ultrashort pulses near 1300 nm and near 1550 nm [15, 16], buried silicon nitride waveguides using pulses near 1300 nm [17], or silicon oxynitride waveguides with 1500 nm pulses [18]. The strongest nonlinear parameter and thus SCG requiring low pulse energies can be found in smaller-bandgap or adjustable bandgap materials, e.g. chalcogenides [19, 20], silicon [21–23], and Si-enriched nitride glass [24]. Increasing the nonlinearity via reducing the bandgap is, however, associated with increased nonlinear losses at shorter wavelengths, such as via two-photon absorption.

A waveguide platform with highest relevance is stoichiometric SiN (Si_3N_4) grown with low pressure chemical vapor deposition (LPCVD), because here a large variety of additional functionalities is available with wafer scale fabrication. These functionalities are based on the accessibility of an extremely wide wavelength range (from the blue, across the visible into the infrared) and that, providing different types of waveguide cross sections [25] and tapers [26], enable, e.g., polarization control, efficient fiber coupling, or bandwidth narrowing with hybrid-integrated diode lasers [27, 28]. The intrinsic absorption and scattering is weak [29] which offers exceptionally low propagation loss, below 0.001 dB/cm for standard waveguides [30]. The latter is central for narrowband spectral filtering and optical delay lines as in quantum optical systems [31], in microwave photonic filters [32, 33] or in programmable optical processors [34]. Finally, as Si_3N_4 has negligible Raman gain, highly coherent supercontinua can be generated using low pump energies [35]. So far in this platform SCG has been mainly investigated with a relatively short pump wavelength around 1 μm, yielding spectral coverage mainly at shorter wavelengths from the blue and across the visible into the near infrared [35–38] .

Here, we demonstrate a significant spectral widening of SCG towards the mid-infrared range.

Optics EXPRESS

This was achieved with a longer pump wavelength in the 1.5 μm telecom range in combination with dispersion engineering based on appropriate cross sections for the fabricated waveguides. These were designed to shift anomalous dispersion towards longer wavelengths, including the 1.5 μm telecom wavelength range. The output spectra extend from about 526 nm to well beyond 2.6 μm, the limit of our detection instruments, thereby spanning at least 2.2 octaves, which is more than 454 THz at the -30 dB level. The spectra broaden towards the mid-infrared with an increasing width of the waveguides, in agreement with modelling.

2. Experimental setup

For enabling SCG with the available pump wavelength of 1560 nm, appropriate dimensions of the waveguide core have to be chosen such that anomalous dispersion, i.e., negative group velocity dispersion (GVD), is imposed broadly around that wavelength. Anomalous dispersion is characterized by a positive value of the dispersion coefficient, $D(\lambda) = -\lambda/c \cdot n''(\lambda)$ [39], where λ is the vacuum wavelength, c is the speed of light, and $n''(\lambda)$ is the second derivative of the effective refractive index of the propagating mode with respect to the wavelength. We used a full vectorial finite-element solver (Fimmwave, Photon Design) to calculate the effective refractive index $n(\lambda)$ as function of wavelength and then derived $D(\lambda)$. The two-dimensional step-index profile used for modelling was based on the actual, somewhat rounded, shape of the waveguide core as resulting from the fabrication process and obtained from scanning electron microscope images of the waveguide cross section [36, 40]. The material dispersion of stoichiometric silicon nitride and silica was taken from [41].

Figure 1 shows the calculated dispersion coefficient *vs.* the wavelength for waveguides of various different widths between 0.7 and 1.3 μm, having the same height (0.9 μm). The calculations imply that anomalous dispersion ($D > 0$) can be obtained over wide spectral ranges including the pump wavelength at 1560 nm if the waveguide core is chosen wider than approximately 0.8 μm. The calculations also show that increasing the waveguide width shifts the range of anomalous dispersion noticeably towards the mid-infrared range, which is expected to shift SCG to longer wavelengths as well.

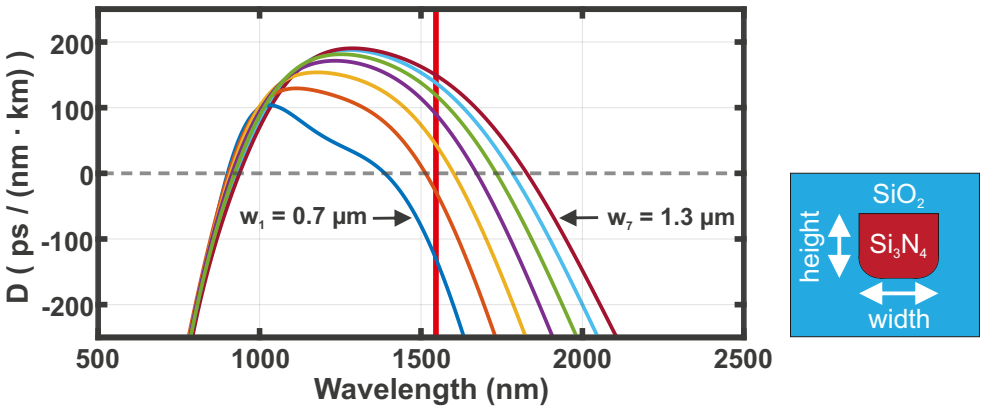

Fig. 1. Calculated dispersion coefficient, $D(\lambda)$, for the fundamental TM-mode in Si_3N_4 waveguides with a height $h = 0.90$ μm and widths varied from $w_1 = 0.70$ μm to $w_7 = 1.3$ μm in steps of 0.1 μm. Anomalous dispersion is present above the dashed zero-dispersion line. The center wavelength of the pump laser at 1560 nm is indicated as red vertical line.

Figure 2 shows the experimental setup used for SCG based on a standard mode-locked erbium fiber laser (Toptica, FemtoFiber Pro). The laser provided ultrashort pulses at a center wavelength

Optics EXPRESS

of 1560 nm, a repetition rate of 40 MHz, and a maximum average output power of 300 mW (maximum pulse energy 7.5 nJ). The pulse duration was about 120 fs (full width at half maximum, FWHM), with a time-bandwidth product of 0.75, as measured with a home-made frequency resolved optical gating (FROG) autocorrelator. A combination of two half-wave plates (HWP) and a polarizing beam splitter (PBS) was used to control the power and the polarization of the beam. Two silver mirrors and an aspheric lens (NA = 0.55 at 1550 nm) were used to steer and focus the beam into the waveguides, respectively. Several Si_3N_4 chips were available as diced with a wafer saw, each chip carrying a set of 100 waveguides with various widths at a pitch of 20 μm and a fixed length of 6 mm.

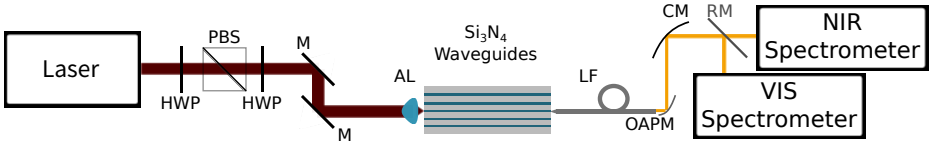

Fig. 2. Schematic view of the experimental setup for supercontinuum generation (SCG) with ultrashort pulses from a mode-locked erbium fiber laser. The pulses enter the Si_3N_4-waveguide sample via two half-wave plates (HWP), a polarizing beam splitter (PBS) and an aspherical lens (AL). A lensed fiber (LF) and an off-axis parabolic mirror (OAPM) collect and collimate the generated SC. A curved mirror (CM) focuses the beam via a removable mirror (RM) into two different optical spectrum analyzers.

In order to determine the waveguide-internal power, the incident average power was measured in front of the first lens and the transmitted power was measured behind a second aspheric lens (NA = 0.55) that collected the radiation behind the waveguide. A low input power was used to avoid spectral broadening. Also, to ensure that only light exiting from the waveguide was measured, and not any light scattered or guided between the SiO_2 cladding and Si bulk, the measurements were performed in the well-collimated part of the output beam, at a distance of about a meter behind the second lens. After optimizing the input and output coupling, typically -8.8 dB $\pm$ 0.6 dB of the incident power was transmitted through the waveguides. To determine the input coupling loss for each of the differently wide waveguides used, we subtracted from each measured transmission value the waveguide-internal propagation loss and output coupling loss. We have taken the propagation loss of the waveguides to be in the order of -0.5 dB/cm as based on previous measurements [40]. This corresponds to a total propagation loss of -0.3 dB for the 0.6 cm long waveguides used here. As output coupling loss we took the Fresnel loss at the output facet (-0.4 dB) and the truncation loss at the second aspheric lens (-2.6 dB) calculated from the almost Gaussian mode field emerging from the waveguide and the aperture of the lens. As a typical example, with the 1 μm wide waveguide, where a transmission of -8.7 dB was measured, we obtain an input coupling loss of -5.4 dB which corresponds to an input coupling of about 29 % of the incident power. This value can likely be increased with improved mode matching.

After the power throughput measurements, in order to conveniently record the spectral distribution of SCG, the second lens was removed and replaced with a lensed fiber. The fiber output was collimated with an off-axis parabolic mirror and focused by a curved mirror via a removable mirror into two optical spectrum analyzers (OSAs) operated in parallel. For the shorter wavelengths, from 380 nm to 1680 nm, an OSA was used with a high dynamic range due to a low dark current (AQ1425 from ANDO, resolution 2 nm). For longer wavelengths, between 1200 nm and 2584 nm, a second OSA was available (NIRQuest 512 from OceanOptics, resolution 6.3 nm). The latter makes use of a CCD-array and thus shows a higher level of dark counts that was subtracted from the recorded spectra. The recordings with the first OSA did not require subtraction. Within their overlap range the spectra of the two OSAs displayed the same shape. We used the agreement to merge the OSA spectra, at a wavelength of 1550 nm, such that

Optics EXPRESS

each supercontinuum spectrum is displayed as a single curve. To enable a direct comparison, all spectra were normalized to their peak values. Employing waveguides with seven different widths and the same height (0.9 μm) we measured the spectral power density of the generated output *vs.* the pump pulse energy incident on the aspheric lens in a range between 0.3 and 6.8 nJ, which corresponds to about 100 pJ to 2 nJ of waveguide-internal pulse energy.

3. Experimental results

Figure 3(a) shows a series of measured spectra as obtained with a 1 μm wide waveguide. This particular example is shown here because all of the main spectral features still lie within the spectral range observable with our pair of OSAs.

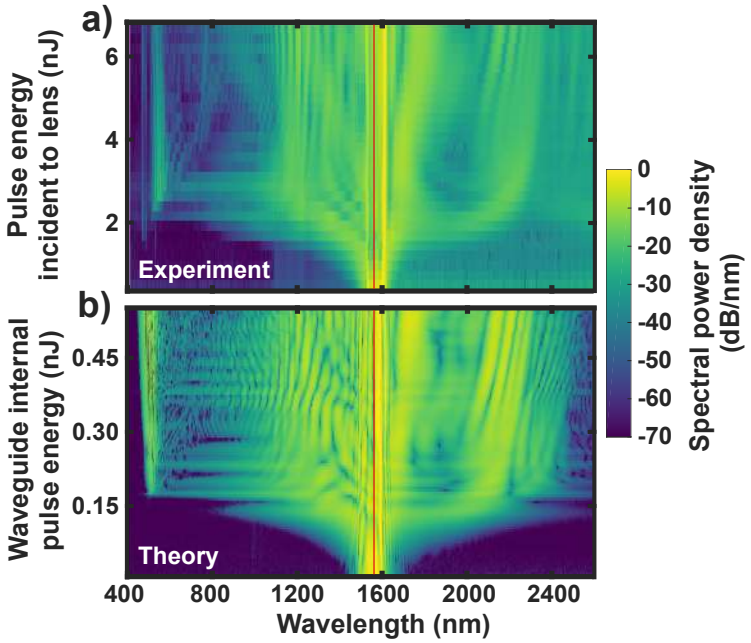

Fig. 3. **a)** Measured spectral power density (color-coded) obtained from supercontinuum generation in a 0.9 μm high and 1 μm wide Si_3N_4 waveguide, using ultrashort pulses (120 fs) from an erbium fiber laser at 1560 nm. The nominal pump wavelength is indicated by the vertical red line. The spectra are displayed *vs.* the pump pulse energy incident on the aspheric lens (upper vertical axis), of which about 29 % was coupled into the waveguide. Each spectrum is normalized to its peak value. **b)** Theoretical spectral density *vs.* waveguide internal pulse energy (lower vertical axis) as obtained from simulations with the experimental values of the waveguide parameters.

It can be seen that the recorded spectra display all well-known features that are typical for SCG as described to large detail, e.g., in Ref. [1]. At the lowest recorded energy the output spectrum already starts to deviate from the incident pump laser spectrum (as retrieved from FROG traces), as is apparent from the two peaks induced by self-phase modulation at 1520 and 1590 nm. The asymmetry in the spectral power density of the two peaks is caused by a slight spectral asymmetry in the pump spectrum. With increasing incident pulse energy, up to 1.8 nJ, there is a spectrally symmetric, steady and steepening increase in bandwidth which indicates increasing self-phase modulation in the waveguide. Approximately at 2.3 nJ, the spectrum reaches almost its maximum bandwidth extending from about 515 nm to 2250 nm at a -30 dB level. The central part of the spectrum, between 1170 and 1750 nm at - 20 dB level, can be addressed to soliton

Optics EXPRESS

dynamics because its extent agrees well with the expected range of anomalous dispersion (900 to 1700 nm as seen in Fig. 1 required for soliton formation. Such dynamics are also apparent from an increasing number of finer spectral features that separate and shift away from the pump wavelength with increasing energy, indicating fission into lower-order solitons. Starting with 1.8 nJ, at the outer edges of the spectrum there appear additional features with narrower bandwidths located at about 520 nm, and located in the wavelength region from approximately 2050 nm to 2270 nm. These features reveal the generation of dispersive waves by solitons (Cherenkov radiation), due to their smaller spectral width and because their wavelengths lie fully within the range of normal dispersion ($D < 0$). At further increased energy of the pump pulses, beyond about 3.5 nJ, the increase in spectral bandwidth with pulse energy is weaker and can be addressed mainly due to a Kerr-induced red-shift of phase matching for the long-wavelength dispersive wave to about 2300 nm, as we find little to no shift in the short-wavelength dispersive wave at about 520 nm.

4. Numerical simulations

For comparing the measured spectra with calculations, we modeled the pulse propagation with the generalized nonlinear Schrödinger equation (GNLSE) as described to more detail in our previous work [42]. The motivation is to determine and verify input parameters that properly calibrate the model. This is important because the nonlinear optical properties of waveguides fabricated with the present material platform have not been fully characterized.

Specifically, there is little information on the Kerr index of LPCVD-grown Si_3N_4. The only information available so far has been given by Levy [43] who derived the Kerr index from measuring the spectral broadening induced by self phase modulation. He reported a value of $(1.1 - 1.2) \times 10^{-15}$ cm^2W^{-1}. Another value, which is often used in simulations, has been reported by Ikeda *et al*., $2.4x10^{-15}$ cm^2W^{-1} [44], albeit for a differently fabricated material, i.e., using a lower-temperature, plasma enhanced growth technique (PECVD). Another concern is that in [44], Ikeda *et al*. did not specify the Si-to-N atomic ratio , leaving open whether the material was stoichiometric. These dissimilarities are important because PECVD-grown silicon exhibits an increased absorption at around 1.5 μm wavelength, where also the Kerr-measurements were performed. Other dissimilarities are a higher pinhole density and a higher hydrogen content [45]. These properties not only lead to higher loss and scattering but should also induce a higher nonlinearity as compared to LPCVD material. Specifically deviations from stoichiometric growth can strongly increase the nonlinearity as found for enrichment with Si [46].

For definiteness in the simulations and for retrieving more information on the Kerr index of LPCVD-grown Si_3N_4 via comparison with experimental spectra, we preliminary use the Kerr index given by Ikeda et al. [44]. The size of the effective modal area, A_{eff}, was calculated with the finite element solver along with the waveguide dispersion as described above which results in a nonlinear coefficient γ of 1.01 $W^{-1}m^{-1}$. The dispersion was included to high precision, up to the 19th order. A contribution from stimulated Raman emission to the nonlinearity was neglected, in view of previous experiments with SCG in silicon nitride waveguides [17, 47]. A shock term was included to model the frequency dependence of the nonlinear index and of the effective modal area [48]. For the 1.0 μm x 0.9 μm-sized waveguides, e.g., we calculated a shock time scale of 1.9 fs. The propagation loss was taken to be 0.5 dB/cm [40]. As the input pulse we took the experimental power and phase spectrum as measured with FROG. We note, that our modelling does not rely on any adjustable fit parameters. This is different from, e.g., [49], where the waveguide dimensions were adjusted to fit the simulations to experimental spectra.

Figure 3(b) displays a series of 100 calculated supercontinuum spectra *vs.* increasing waveguide-internal pump pulse energy, assuming the same waveguide width (1 μm) and height (0.9 μm) as used for the measurements. It can be seen that there is a very good agreement of the spectral distribution with the experimental data. One can recognize essentially the same spectral

Optics EXPRESS

development *vs.* increasing pulse energy, from self-phase modulation towards soliton formation and fission. The agreement suggests that the characteristic length of nonlinear interaction, the dispersion length (strength of anomalous dispersion) and detailed shape of waveguide dispersion contained in higher order terms are appropriately described within the anomalous range. We note that also the spectral positions of the long and short-wavelength dispersive waves are predicted with high agreement, with only a small offset for the low-wavelength edge of the SC. This discrepancy is attributed to a small difference in material dispersion at the short wavelengths. This implies that phase matching was modeled with proper dispersion in the outer, normal dispersion range (especially for the longer wavelengths), including a proper group velocity of the solitons that excite dispersive waves. Finally, also the spectral Kerr shift of the dispersive waves, here mainly at the long-wavelength side, is matching well the experiments. The overall agreement, specifically the absence of self-frequency shifting, confirms that neglecting stimulated Raman scattering is justified here. We note that the absence of Raman contributions is a main advantage as compared to SC generation in optical fibers where such non-parametric contributions may introduce noticeable shot-to-shot incoherent output. Furthermore, from the absence of Raman scattering a coherent supercontinuum is expected [35]. We have confirmed coherent generation explicitly with calculation of the shot-to-shot coherence for the supercontinua presented in Fig. 3. We found a near unity degree of coherence for the entire spectral range that has a larger than -30 dB relative spectral power density. This result is in agreement with our previous calculations where neglecting Raman scattering was also justified [36] and where pumping at 1 μm wavelength showed near unity pulse-to-pulse coherence as well [50]. By spectrally integrating the output and comparing with the internal pump pulse energy we observe that the calculated waveguide-internal conversion efficiency is very high, typically about 93 %, due to the absence of Raman conversion and due to low waveguide propagation loss.

As the next step, based on high agreement between the simulated measurements spectral distributions, we also compare the waveguide-internal pulse energies required for SCG in the experiment with those predicted by the calculations. As described above, we have concluded from throughput measurements and loss estimates that typically 29 % of the incident power is coupled into the waveguide (input coupling loss -5.4 +/- 0.6 dB). For an unambiguous comparison of pump energies we chose the onset of the dispersive wave at the shorter wavelength side of the spectrum. In the experiment the dispersive waves occurs at around 2.1 nJ of incident energy, corresponding to about 0.61 nJ internal energy. Compared to this, in the simulations the dispersive wave generation sets in already at 0.17 nJ, which is a factor 3.6 lower.

In order to identify possible reasons for this deviation we inspected several effects. A relatively large uncertainty is usually present regarding the input coupling loss. Here, however, transmission measurements provide a lower bound for these losses. Underestimating losses in the waveguide, output coupling or truncation at the second lens would rather increase the estimated value for input coupling. A slight misalignment of the input coupling with increasing pump power was observed. We conclude this from a slightly sub-linear growth of the wavelength-integrated OSA spectra *vs*. incident pump power, spanning from the low-power values used for transmission experiments towards the higher-power for SCG . However, these measurements limit an underestimation of the input coupling to a factor of 1.3 at most. Another source of error might have been pump energy coupled into higher-order modes, which have a different dispersion and, therefore, do not contribute to the SCG. However, input coupling to higher-order modes has been experimentally investigated with great care showing that such coupling can safely be neglected for our experimental conditions. Similarly, measuring the transmitted power in the collimated beam far behind the output lens rules out that the transmission measurements are impaired by light which was not coupled into the waveguide but still scattered or guided in the SiO_2 cladding towards the output facet. In the model, a source of error might have been an underestimated size of the mode field area, via underestimating the waveguide cross sectional area, which overestimates the

Optics EXPRESS

nonlinear coefficient. However, the very good spectral agreement of the calculated and measured spectra indicate that the waveguide dispersion was modeled correctly, which rules out a wrongly assumed waveguide cross section. Our overall conclusion from these considerations is that the nonlinear refractive index used in the simulations is larger than in the waveguides that we have experimentally investigated. Quantitatively, the nonlinear refractive index for our waveguides appears to be about 3.6-times smaller than the previously reported value for PECVD-grown silicon nitride [44] and about 1.8-times smaller than the value reported for LPCVD-grown Si_3N_4, which is obtained from SPM-induced spectral broadening [43]. A further clarification might be obtained by repeating the power modulation experiments in [44] with LPCVD-grown Si_3N_4 waveguides.

5. Dependence on waveguide width

In order to extend the supercontinuum further towards the mid-infrared side of the spectrum, we recall that the long-wavelength zero-dispersion wavelength in Fig. 1 shifts to lager values with increasing waveguide width. The dispersive waves result from a coherent energy transfer from the soliton in the anomalous dispersion regime to phase-matched frequencies in the normal dispersive regime, where the phase matching depends on the phase- and group velocity of the soliton as well as its peak power [1, 51, 52]. This suggests that the infrared side of the SC would shift to longer wavelengths as well. For a verification we carried out spectral measurements *vs.* increasing waveguide width. Figure 4 shows the spectral power density recorded with seven different widths (from 0.7 to 1.3 μm) at the same, maximum available pump pulse energy of 6.8 nJ incident on the aspheric lens.

The dotted line indicates the change of the -30 dB limit at the long-wavelength side of the spectrum. It can be clearly seen that the infrared end of the spectrum extends progressively towards mid-infrared wavelengths with increasing waveguide width. The observable wavelength shift is about 2.45 nm per nm waveguide width. A further progression and extension of the spectra to wavelengths beyond 2.6 μm seems present for the three widest waveguides (1.0 to 1.3 μm) as well, but could not be recorded with the available spectroscopic equipment. Our theoretical model predicts the SC extending to wavelengths of 2.6, 2.7, 2.8 and 2.9 μm for waveguide widths of 1.1, 1.2, 1.3 and 1.4 μm, respectively, while reproducing the experimental value for the smaller widths. The shift in location of the long-wavelength dispersive wave is reduced to about 1 nm per nm waveguide widening for widths larger than 1.1 μm.

The widest of all generated spectra, within the available detection range, was obtained with a 1-μm wide waveguide and a pump pulse energy incident on the aspheric lens of 4.7 nJ (1.4 nJ waveguide internal). The spectrum is displayed in Fig. 5. From its short-wavelength -30 dB-edge at 526 nm it extends to at least 2.584 μm (mid-infrared end of OSA detection range), which corresponds to a bandwidth of more than 454 THz and spans at least 2.2 octaves.

6. Summary and conclusions

In summary, we have demonstrated extremely wide bandwidth of supercontinuum generation in stoichiometric Si_3N_4 waveguides, using a standard erbium-doped fiber pump laser that provided ultrashort pulses in the telecom wavelength range at 1560 nm. In a 6 mm long waveguide with a core area of 1.0×0.9 μm^2 and pumped by 120 fs long pulses with a pulse energy of 4.7 nJ incident on the aspheric lens, the supercontinuum radiation showed a spectral bandwidth of more than 454 THz, spanning at least 2.2 octaves, from the visible at 526 nm to the mid-infrared (beyond 2584 nm). The shapes of the generated spectra are in very good agreement with theoretical modelling via numerical integration of the generalized nonlinear Schrödinger equation (GNLSE). Based on this agreement a comparison of the required waveguide-internal pump pulse energy in the simulation and the measurements has been performed. The comparison revealed a factor of 3.6 lower pulse energy required in the simulations. A careful analysis suggests that the

Optics EXPRESS

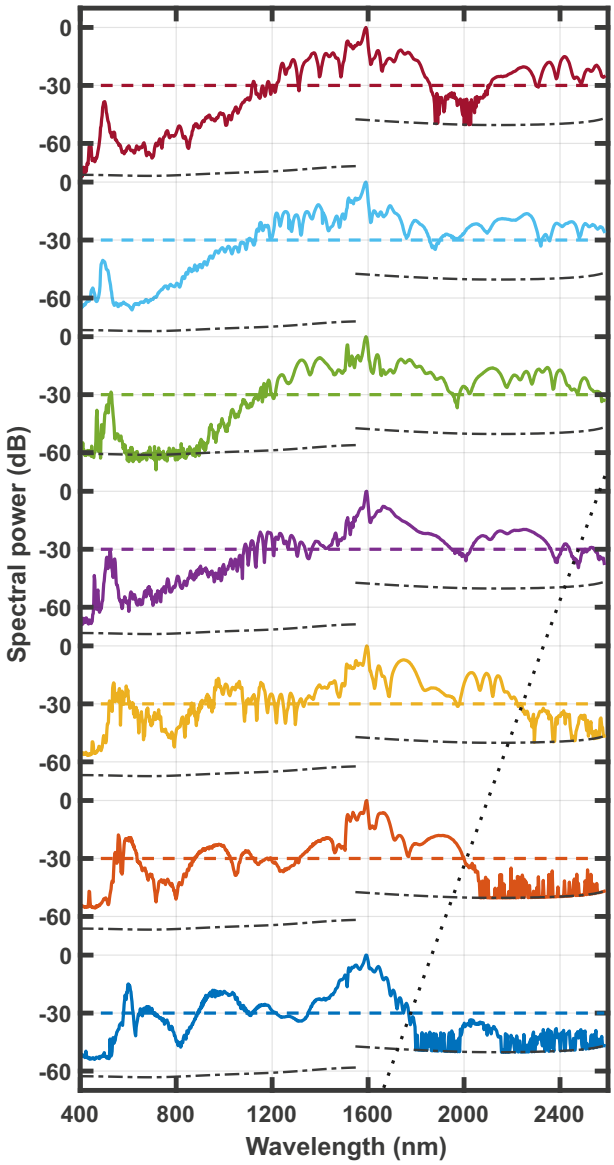

Fig. 4. Measured spectral power density of supercontinuum generation using seven different waveguide widths, increasing from (blue trace) 0.7 μm (blue trace) to 1.3 μm (red trace) in steps of 0.1 μm, pumped with the same, maximum available pump pulse energy of 6.8 nJ incident on the aspheric lens. For clarity the peak values of all spectra are normalized to 0 dB and vertically offset by 80 dB with respect to each other. The horizontal dashed lines mark the respective -30 dB levels. The dash-dotted curves show the average noise levels for the short-wavelength OSA, and a baseline after dark-count subtraction for the long-wavelength OSA. The straight dotted line shows that the -30 dB infrared-end of the spectra tunes towards the mid-infrared range with increasing width of the waveguides.

Optics EXPRESS

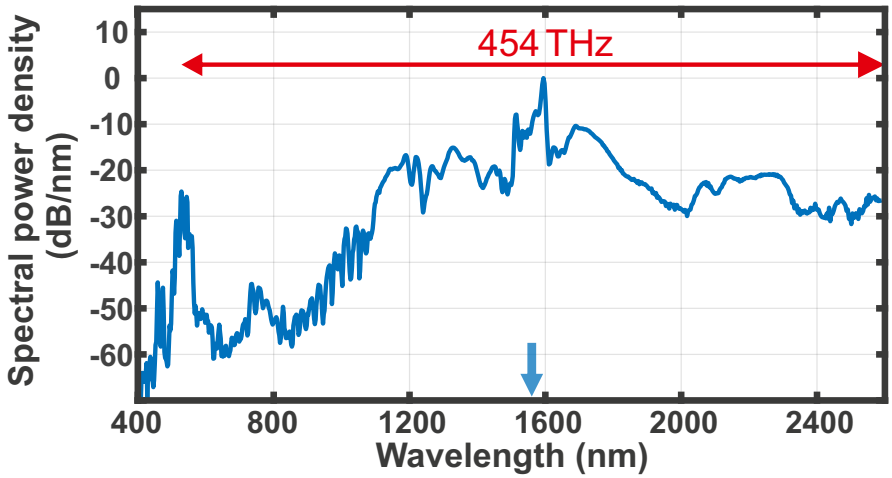

Fig. 5. Supercontinuum spectrum generated in a 1 μm wide and 0.9 μm high waveguide using a pump pulse energy of 4.7 nJ incident to the aspheric lens (in-coupled pulse energy 1.4 nJ). The pump wavelength of 1560 nm is indicated with an arrow. From the short-wavelength -30 dB-edge at 526 nm the spectrum extends to at least 2584 nm (mid-infrared end of OSA detection range). This corresponds to a spectral bandwidth of more than 454 THz and spans more than 2.2 octaves.

nonlinear refractive index of LPCVD-grown stoichiometric silicon nitride, Si_3N_4, is smaller by a factor of about 3.6 than the previously reported value for PECVD-grown silicon nitride [44] and smaller by a factor of 1.8 than the previously reported value for LPCVD-grown Si_3N_4 [43]. A further clarification should be attempted, such as with direct index modulation experiments using LPCVD-grown Si_3N_4 waveguides.

Shifting the long-wavelength edge of the supercontinuum generation towards the mid-infrared with increasing waveguide width was achieved in agreement with engineering the waveguide dispersion. In the experiment a wavelength shifting of 2.45 nm per nm waveguide width of the -30 dB level at the infrared-side of the spectrum was observed, for waveguide widths between 0.7 μm and 1.0 μm. We note that following our primary report on mid-infrared shifting [53] there was a subsequent observation [54] analogous to our results. Furthermore, the high index contrast provides tight guiding which concentrates the optical mode predominantly in the Si_3N_4 core, where mid-infrared absorption is weaker [55]. The results imply that highly efficient supercontinuum generation appears feasible, if a low-loss input coupling can be obtained. We conclude this from the consistency between transmission loss measurements and detailed loss estimates, as well as from the good agreement between the shape of the measured and numerically calculated spectra. In these calculations only a low propagation loss and a negligible Raman conversion were assumed, thereby yielding a waveguide-internal conversion efficiency of typically 93 %. The measurements presented here, in agreement with mode matching calculations, show that the input coupling may be substantially increased by combining tighter focusing and tapered waveguides [26, 56]. With these properties and options, stoichiometric silicon nitride waveguides pumped with mode-locked telecommunication laser sources provide an interesting platform for various applications, including multiple-octave spanning frequency combs with self-referencing for frequency metrology [57] or mid-infrared dual comb spectroscopy [58].

Optics EXPRESS

Funding

NanoNextNL (6B-Functional Nanophotonics) a micro and nanotechnology consortium of the Government of the Netherlands and 130 partners.
Dutch Technology Foundation STW (11358) which is part of the Netherlands Organization for Scientific Research (NWO), and which is partly funded by the Ministry of Economic Affairs.

Acknowledgments

We thank Albert van Rees (Xio Photonics B.V.) for designing the lithography mask and Richard Mateman (LioniX International B.V.) for cleanroom processing and fabrication of the samples.